ACS OMEGA

http://pubs.acs.org/journal/acsodf

Article

Adsorption of NO_x (x = 1, 2) Molecules on the CoFeMnSi(001) Surface: First-Principles Insights

Muhammad Mushtaq,* Norah Algethami, Muhammad Abdul Rauf Khan, Ahmad I. Ayesh, Muhammad Mateen, Amel Laref, Shaimaa A. M. Abdelmohsen,* and M. Khalid Hossain

Cite This: *ACS Omega* 2023, 8, 14005−14012

Read Online

ACCESS | Metrics & More | Article Recommendations

ABSTRACT: In this article, the adsorption of NO_x (x = 1, 2) gas molecules on the (001) surface of CoFeMnSi quaternary Heusler alloys has been investigated theoretically with density functional theory (DFT) calculations. The adsorption strength was estimated with adsorption energy (E_a), magnitude of charge transfer (ΔQ), charge density difference (CDD), minimum distance between molecule and surface (d), and adsorption mechanism was analyzed with density of states. The results showed that unlike half-metallic nature of the bulk phase, the pristine CoFeMnSi(001) surface exhibited metallic character caused by the emergence of electronic states of the atoms in the top-most layer of the surface. It was found that both NO and NO_2 molecules undergo chemical adsorption and strongly interact with the surface evidenced by the large value of E_a and ΔQ. In particular, the NO_x molecule dissociates into N and O atoms for some adsorption configurations. Bader charge analysis reveals that NO_x molecules act as charge acceptors by drawing charge from the surface atoms through p−d hybridization. Such findings might be useful in the development of Heusler alloys based gas sensors.

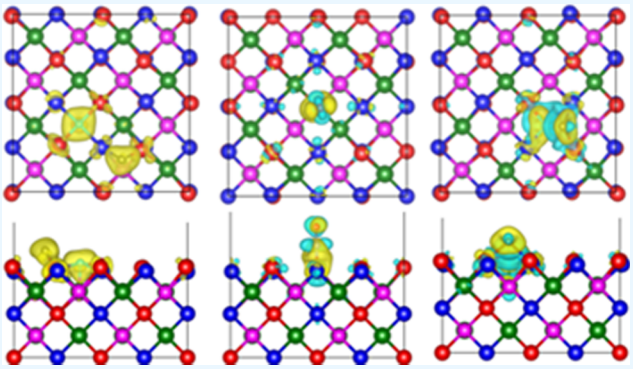

1. INTRODUCTION

Heusler alloys may exhibit metallic, semi metallic, or semiconducting properties with different crystalline structures.[1] The electronic structures of such alloys could be designed by elemental substitution which enables tuning their functional characteristics.[2] Equi-atomic quaternary Heusler alloys with a general formula ABCD and stoichiometry of 1:1:1:1 have received much attention recently due to their extraordinary properties.[3] The spin-gapless semiconductor Heuslers have zero band gap for the majority electrons while they have non-zero band gap for the minority electrons; thus, they can be utilized for multiple applications including spintronic devices.[4] Devices based on these alloys have low power dissipation than the pseudo ternary alloys because of the lower length of spin diffusion.[5]

Transition metals are known for their catalytic properties that are dominated by multiple factors such as electronic structures, surfaces, and defects. Alloying of metals modifies their atomic configuration that can lead to changes in the catalytic characteristics. The CoFeMnSi quaternary Heusler alloy has been reported to exhibit three lattices that are nonequivalent depending on the Co, Fe, Mn, and Si occupancy within the Wyckoff coordinate.[5] Accordingly, CoFeMnSi may crystallize in either of three structures (Y-type).

Recently, Mishra et al. investigated thin films based on CoFeMnSi Heusler alloys by examining their structural, magneto transport, magnetic, and charge transport features.[5] They suggested effective contribution of skew scattering that is phonon-related; thus, both carrier concentration as well as mobility were approximately temperature-independent. Ilkhani et al. investigated the electronic, magneto-optic, and magnetic properties of CoFeMnSi and CoFeMnAs Heusler alloys using density functional theory computations.[4] The results showed the highest magnitude for Kerr rotation by 0.21° and 0.12° assigned to CoFeMnAs and CoFeMnSi alloys, respectively. Mebed et al. examined the adsorption of CO gas on the (001) surface of CrCoIrGa Heusler alloy using DFT computations.[6] The observed adsorption energy values along with charge transfer and the adsorption length predicted strong chemisorption of CO on the (001) surface which may be utilized for gas sensor applications. Kojima et al. explored Heusler alloys

Received: January 28, 2023
Accepted: March 2, 2023
Published: April 4, 2023

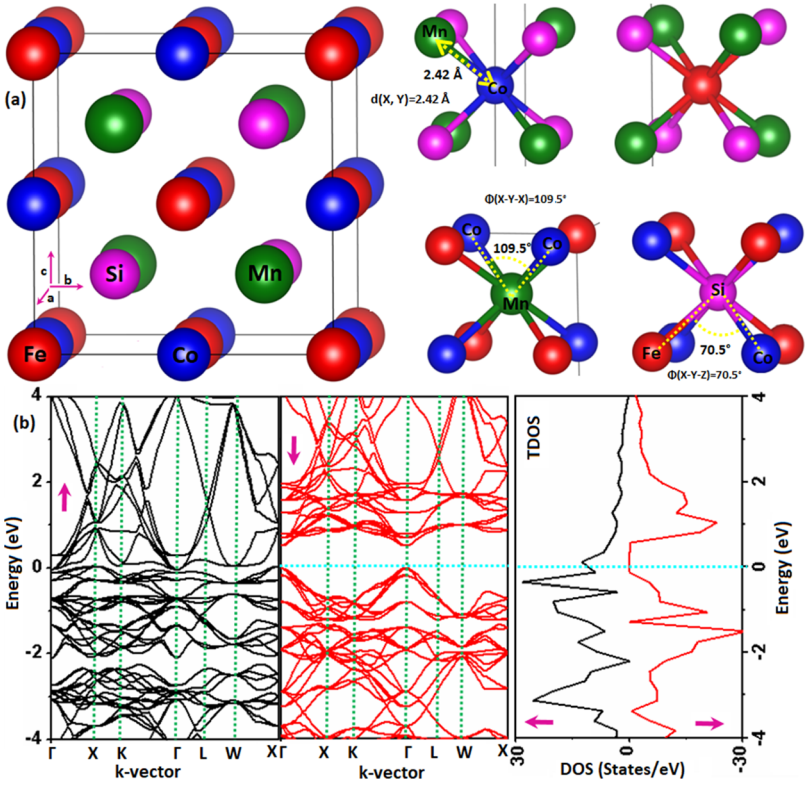

Figure 1. (a) Atomic structure, (b) band structure, and density of states of the bulk CoFeMnSi Heusler alloy.

for propyne hydrogenation as well as carbon monoxide oxidation. Co_2FeGe revealed greater activity than the pristine Co element for propyne hydrogenation, and neither Ge nor Fe showed clear activity.[2] For carbon monoxide oxidation, most of the alloys presented clear activity. Hence, the interaction strength of Heusler alloys toward adsorbates can be tuned by using the appropriate combination of elements. They also demonstrated in a separate study[7] a systematic way for tuning the adsorption properties by fractional substitution with new elements.

Emission of nitrogen oxides is normally correlated to energy consumption and emission of co-emitted gases, along with the release of greenhouse gases.[8] NO and NO_2 are usually released as a result of fossil fuel combustion, and they react with ozone, causing photolysis of NO_2.[9] This is normally converted to either nitrates or nitric acid, extracted through wet and dry processes from the atmosphere. Furthermore, NO and NO_2 contamination of the environment generates severe consequences, for example, smog, acidic rain, damage of the ozone layer, and well-known global warming.[10] Therefore, to reduce and control such issues, the development of NO_x-based sensors is highly desirable. Several efforts have been devoted for the design of high sensitive and selective materials and methods for the detection of NO_x gases.[11−15]

The main objective of this work is to explore the suitability of Heusler alloy CoFeMnSi for the sensing of toxic gases emitted from multiple sources, which may result in severe environmental and health issues. Herein, the adsorption of NO and NO_2 molecules on the (001) surface of CoFeMnSi quaternary Heusler alloy is explored by means of density functional theory calculations. The adsorption of gas molecules is evaluated by the quantification of adsorption energy, charge transfer, and modifications in electronic properties, along with charge density difference.

2. COMPUTATIONAL METHODS AND DETAILS

The present study was based on density functional theory (DFT)-based quantum mechanical total energy calculations, performed with Vienna Ab initio Simulation Package (VASP), which uses pseudo-potentials and plane-wave basis set and describes the interaction between electrons and ions with projector augmented wave method (PAW).[16] In its foundation, the standard DFT fails to accurately describe the contribution of electron−electron interactions (due to spins and charge) to the total energy of the system; therefore, the exchange-correlation energy $E_{XC} = KE^{e}_{int} - KE^{e}_{non-int} + PE^{ee}_{int} - PE^{ee}_{H}$ (where KE^{e}_{int}, $KE^{e}_{non-int}$, PE^{ee}_{int}, PE^{ee}_{HF} describe the kinetic energy of interacting electrons, kinetic energy of non-interacting electrons, Coulomb energy for interacting electrons, and Coulomb energy for electrons computed within Hartree−Fock approximation) is calculated with some approximations. In our case, the XC part of the total energy was calculated using generalized gradient estimation (GGA) proposed by Perdew−Burke−Ernzerhof (PBE).[17] The plane waves were expanded with an energy cut-off of 500 eV. Simulations were started from the calculation of the lattice constant, magnetic coupling, and electronic properties of bulk CoFeMnSi. The bulk unit cell was relaxed with a mesh of 10 × 10 × 10 k-points, and the density of states was computed using a relatively dense mesh of 12 × 12 × 12 k-points. To obtain the (001) surface, the relaxed structure of bulk CoFeMnSi was cut in a direction normal to the c-vector of the unit cell and a two-dimensional slab model of the surface was obtained by setting a vacuum level of about 15 Å in the *z*-direction, which ensures that there is no interaction between the periodically repeating surfaces along the *z*-direction. The (001) surface of CoFeMnSi was composed of five atomic layers such that during the relax process, the bottom three layers were kept fixed at a bulk

https://doi.org/10.1021/acsomega.3c00569
ACS Omega 2023, 8, 14005−14012

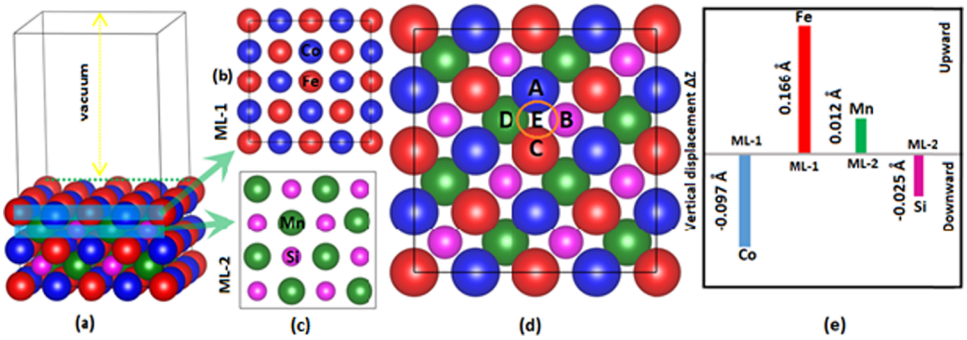

Figure 2. (a) Relaxed geometry of the (001) thin film surface of CoFeMnSi, (b) top view of the first layer (ML-1), (c) top view of the second layer (ML-2), (d) various adsorption sites on the (001) surface, (e) vertical displacement (ΔZ) of atoms in ML-1 and ML-2.

configuration and only the atoms of top two layers were allowed to relax using selective dynamic and a mesh of 2 × 2 × 1 k-points in the Brillouin zone. Other properties including the Bader charge, density of states, and charge density difference were obtained with 5 × 5 × 1 k-points.

The NO_x (x = 1, 2) molecule was first relaxed in the isolated form then placed above the surface at various sites with an initial distance of 1.6 Å from the surface. The long-range van der Waals (vdW) interactions were incorporated in the scheme of dispersion of Grimme (i.e., DFT-D3).[18] The interaction of molecules with the surface was examined by calculating the adsorption energy E_{ads}, adsorption height h, minimum distance between molecule and surface d, charge transfer between the molecule and adsorbent ΔQ, Fermi energy E_F, total magnetic moment M, spin-polarization SP, and charge density difference (CDD) plots. The E_{ads} was calculated using eq 1, given below

$$E_{ads} = E_{(surface+molecule)} - E_{(surface)} - E_{(molecule)} \quad (1)$$

where $E_{(surface\ +\ molecule)}$, $E_{(surface)}$, and $E_{(molecule)}$ represent the total energy of the system of the surface and molecule, total energy of the surface, and total energy of the isolated molecule.

3. RESULTS AND DISCUSSION

3.1. Bulk CoFeMnSi. Figure 1a reveals the relaxed unit cell structure of the bulk CoFeMnSi (CFMS) quaternary Heusler alloy. This compound forms a Y-3 type (prototype LiMgPdSn) face-centered cubic lattice of the F-43m (#216) symmetry. The unit cell of CFMS is composed of four atoms (Co:Fe:Mn:Si = 1:1:1:1) where Co, Fe, Mn, and Si atoms occupy the Wyckoff position 4d(3/4,3/4,3/4), 4a(0,0,0), 4b(1/2,1/2,1/2), 4c(1/4,1/4,1/4), respectively.[19] The subparts of the CFMS unit cell (Figure 1a right panel) have the AB_4 configuration where the element A (Co, Fe, Mn, or Si) is coordinated with four B atoms of different types.

For example, when A = Co, the B atom of the AB_4 unit represents Mn and Si atoms. Owing to the presence of magnetic elements in the given compound, it is important to consider the spin effect in the structure relaxation. Therefore, CFMS is fully relaxed in spin-polarized calculations. The results showed that CFMS has a lattice constant a of 5.598 Å and is ferromagnetic in the ground state. This value of a is in agreement with a value of 5.588 Å reported by Alijani and co-workers.[19] In addition, the average distance between A and B atoms was found to be 2.42 Å, and the B−A−B angles are 109.5° and 70.5°. The ground-state spin-polarized band structure and density of states (DOS) of the CFMS are presented in Figure 1b. Clearly, the band structure of majority

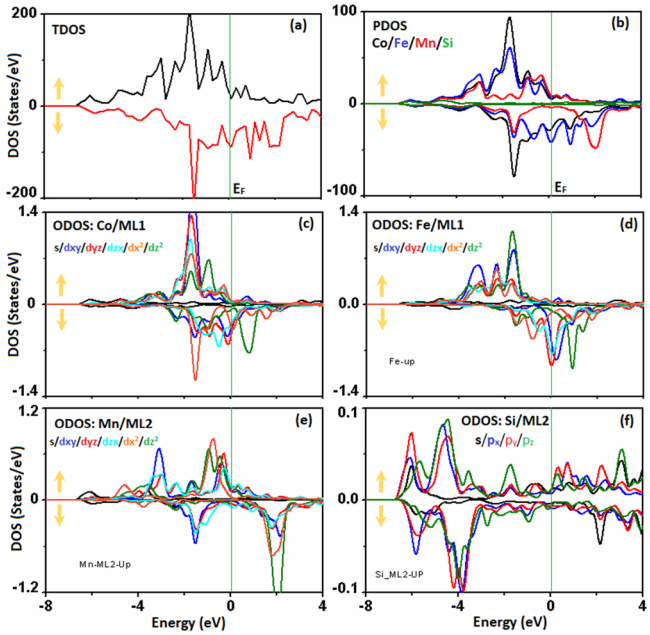

Figure 3. (a) TDOS of the (001) CoFeMnSi surface, (b) PDOS of the constituent Co, Fe, Mn, and Si atoms, (c) orbital DOS (ODOS) of Co atom in ML-1, (d) ODOS of Fe atom in ML-1, (e) ODOS of Mn atom in ML-2, and (f) ODOS of Si atom in ML-2.

electrons and minority electrons is not identical at the Fermi level E_F (0 eV energy level). In the majority electron band structure, the energy bands cross the E_F at multiple values of the k-vector, showing the metallic character of the majority electron states, while the energy band diagram of minority electrons has a distinct band gap (E_g) around E_F. Thus, CFMS is said to be a half-metallic (HM) material, i.e., fully spin-polarized, and it has been reported as HM in the literature as well.[19] The opening of the band gap in the minority bands might be attributed to the splitting of both energy bands (majority and minority) caused by the exchange interaction among the atoms, due to which E_F is shifted above the filled minority energy bands. Furthermore, in the majority electron band structure, the valence band maxima (VBM) and conduction band minima (CBM) are located at the same value of the k-vector, which confirms a direct band gap. The calculated band gap is ∼0.44 eV and the HM gap, which is regarded as the fundamental descriptor of the HM property and is taken as the energy difference between EF and CBM, is also ∼0.44 eV because the valence band top (VBM) also lies at

https://doi.org/10.1021/acsomega.3c00569
ACS Omega 2023, 8, 14005−14012

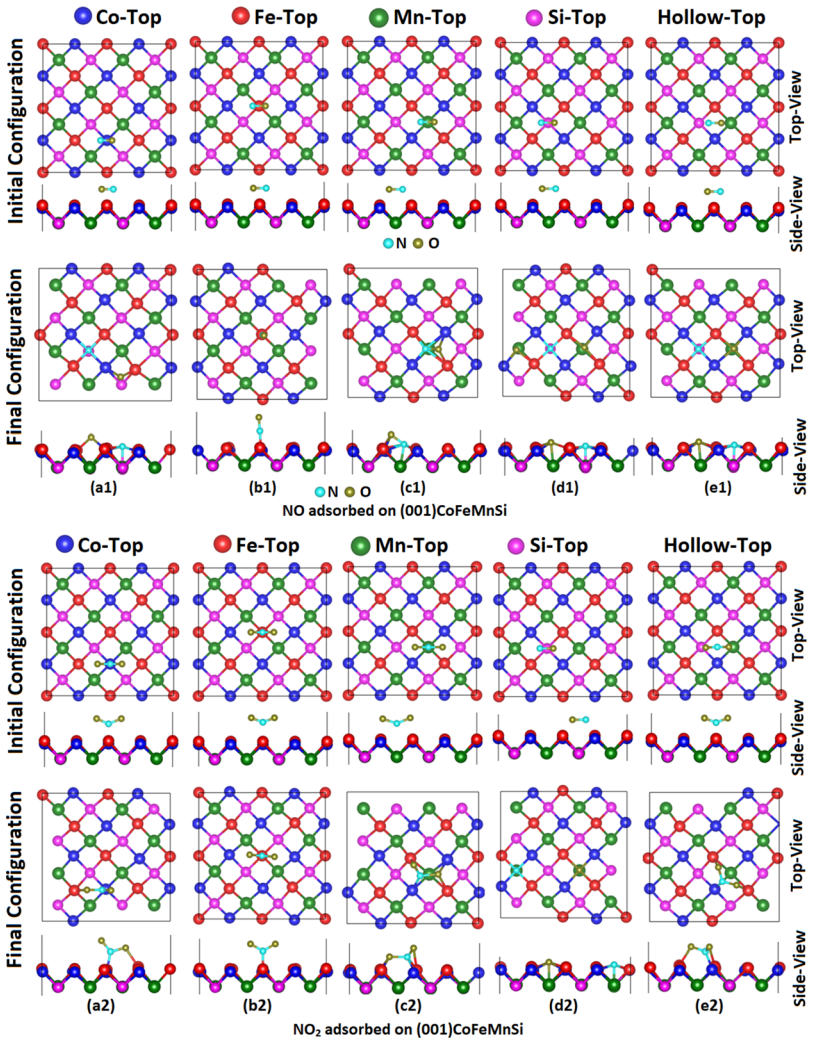

Figure 4. Initial and final (relaxed) configurations of NO and NO_2 molecules adsorbed on the (001) surface of CoFeMnSi. (a1) NO on the top of the Co atom of ML-1, (b1) NO on the top of the Fe atom of ML-1, (c1) NO on the top of the Mn atom of ML-2, (d1) NO on the top of the Si atom of ML-2, (e1) above the hollow site, (a2) NO_2 on the top of the Co-atom of ML-1, (b2) NO_2 on the top of the Fe atom of ML-1, (c2) NO_2 on the top of the Mn atom of ML-2, (d2) NO_2 on the top of the Si atom of ML-2, (e2) NO_2 above the hollow site.

Table 1. Adsorption EnergyE_a (eV), Charge Transfer between Molecule and Adsorbent ΔQ|e| (Negative Value Means Adsorbent Donates Charge to Molecule), Nearest Atom to Atom Distance$d$ (Å), Fermi EnergyE_F (eV), Total Magnetic Moment$M$ (μ_B) and Spin-Polarization SP (%) Calculated at the DFTD3 Level for NO_x Molecules Adsorbed on the (001) Surface of CoFeMnSi[a]

gas	site	E_a	ΔQ	d_{min}	E_F	M	SP	molecule
NO	Co-top	−4.348495	−0.307014	1.78	0.8570	117.91	62.34	dissociated
	Fe-top	−3.184635	−0.404074	1.64	0.8657	118.00	37.07	compact
	Mn-top	−3.492315	−1.244577	1.86	0.8708	119.17	42.47	compact
	Si-top	−6.167045	−2.19991	1.87	0.8885	115.22	9.97	dissociated
	hollow	−5.121935	−2.517358	1.93	0.8956	118.90	38.91	dissociated
NO_2	Co-top	−3.040941	−0.773266	1.82	0.8348	119.85	38.8	compact
	Fe-top	−2.374251	−0.670055	1.84	0.8032	117.72	5.26	compact
	Mn-top	−3.311821	−1.248353	1.93	0.8567	120.18	19.37	compact
	Si-top	−0.079601	−3.593612	1.89	0.9324	119.89	22.91	dissociated
	hollow	−3.460821	−1.030912	1.84	0.8496	120.89	19.85	compact

[a]Pristine (001) surface: M = 121.54 μ_B, E_F = 0.8431 eV, SP = 26.2%.

the E_F. Such phenomena could be utilized for devices based on spin-tunable charge transport phenomena.[1]

3.2. Bare CoFeMnSi(001) Surface. Next, we analyze some basic properties of CFMS in the (001) thin film form. The relaxed structure of the (001) surface of CFMS, is shown in Figure 2. The side view of this figure reveals that the present (001) surface is composed of atomic layers, namely, the first layer (ML-1, the top-most layer, and it is composed of only Co

https://doi.org/10.1021/acsomega.3c00569
ACS Omega 2023, 8, 14005−14012

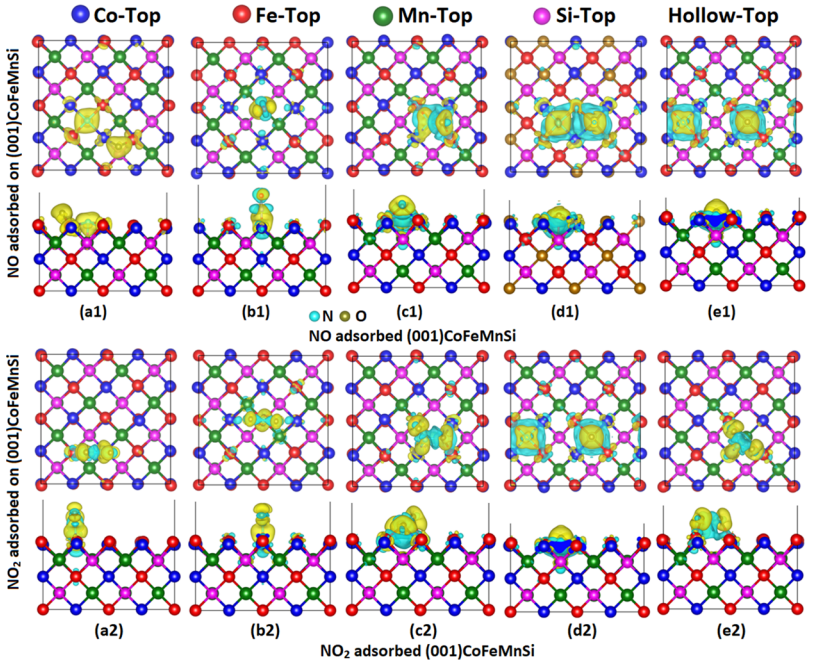

Figure 5. CDD plots of (a1) NO on the top of the Co-atom of ML-1, (b1) NO on the top of the Fe atom of ML-1, (c1) NO on the top of the Mn atom of ML-2, (d1) NO on the top of Si-atom of ML-2, (e1) above the hollow site, (a2) NO_2 on the top of Co-atom of ML-1, (b2) NO_2 on the top of the Fe atom of ML-1, (c2) NO_2 on the top of the Mn atom of ML-2, (d2) NO_2 on the top of the Si atom of ML-2, (e2) NO_2 above the hollow site. Yellow (cyan) region represents charge accumulation (depletion). Plots are visualized at the iso-surface value of 4.0 10^{-3} e/Å^3.

and Fe atoms), second layer (ML-2, the second top-most layer, and it contains only Mn and Si atoms), third layer (ML-3), fourth layer (ML-4), and fifth layer (ML-5). It is well understood that physical and chemical properties of thin film surfaces are mainly controlled by the top-most layers; therefore, we pay particular attention to the structural, electronic, and magnetic properties of ML-1 and ML-2 (and their top views are shown in Figure 2b). The vertical displacement (i.e., along the *z*-axis) of the atoms in ML-1 and ML-2 is shown in Figure 2e, where the positive (negative) sign indicates outward (inward) displacement. It is inspected that in ML-1, Co atoms have 0.097 Å downward and Fe ones have 0.166 Å upward vertical displacements, whereas, in layer ML-2, Mn atoms are displaced by 0.012 Å in the upward direction and Si atoms are displaced about 0.025 Å downward. In addition, due to the presence of vacuum above the ML-1, the atoms of the ML-1 are not fully saturated chemically (i.e., possess dangling bonds) and interact only with intralayer atoms (of ML-1) and interlayer atoms of ML-2. On the other hand, the atoms in ML-2 have a bulk-like environment because they are surrounded by ML-1 atoms and ML-3 atoms. Similarly, the atoms in the middle and bottom of the surface (ML_n, n = 3, 4, 5) have a bulk-like configuration and are fixed at their actual position. Because of such displacements, the local geometry of the surface is changed, and some distortions or reconstructions emerge in the surface, which profoundly affect the actual properties of the bulk counterpart. In order to estimate the effect of surface reconstruction on the electronic properties of CFMS, total, partial, and orbital density of states (TDOS, PDOS, and ODOS) are computed, as shown in Figure 3.

TDOS (Figure 3a) describes the global degree of spin-polarization (SP) in the CFMS (001) surface. Obviously, a considerable population of both majority and minority electronic states is present at E_F, corroborating the metallic nature of the CFMS (001) surface. Thus, the bulk HM property of CFMS is lost in the CFMS (001) surface. The reason behind the HM to metallic transition can be traced with the help of PDOS/ODOS plots. In Figure 3b, it is shown that the electronic states appearing at E_F in the minority spin channel mainly belong to Co and Fe atoms, while Mn and Si atoms have apparently no contribution. The analysis of ODOS plots shows that induced states at E_F in the spin-down channel are dominated by the d_{xy}, d_{yz}, d_{zx}, and d_x^2 orbitals of Co atoms in the ML-1 and d_{xy}, d_{yz}, and d_{zx} orbitals of Fe atoms in the ML-1. In contrast, the Mn and Si atoms have shown no significant role in the formation of energy bands at E_F. The reason for the emergence of Co-d and Fe-d states at E_F is that these atoms (in ML-1 of the surface) have some unfilled d-states which are shifted toward unoccupied higher energy states. That is why, the bulk HM property is lost and CFMS (001) behaves like a weakly spin-polarized material.

3.3. CoFeMnSi(001) Surface with NO_x (x = 1, 2) Molecules. In the following sections, we discuss the adsorption behavior of NO_2 (x = 1, 2) molecules on the CFMS (001) surface. Five possible absorption sites, namely, A-, B-, C-, D-, and E-sites, are shown in Figure 2c.

The A-site lies on the top of the Co atom (in the ML-1), the B-site lies on the top of the Fe atom (in the ML-1), the C-site lies on the top of the Mn-atom (in the ML-2), the D-site is on the top of the Si-atom (in the ML-2), and the E-site is the interstitial hollow site and lies in the middle of all atoms.

Figure 4 reveals the relaxed structures before and after the adsorption of gas molecules on the selected adsorption sites. A gas molecule is placed on each site horizontally at a separation of 1.5 Å from the CFMS (001) surface as can be seen in the side view of the initial configuration. The figure in final configurations reveals that both NO (Figure 4a1−e1) and NO_2 (Figure 4a2−e2) establish bonds with the CoFeMnSi structure at all sites. The local geometry is deformed at the adsorption

https://doi.org/10.1021/acsomega.3c00569
ACS Omega 2023, 8, 14005−14012

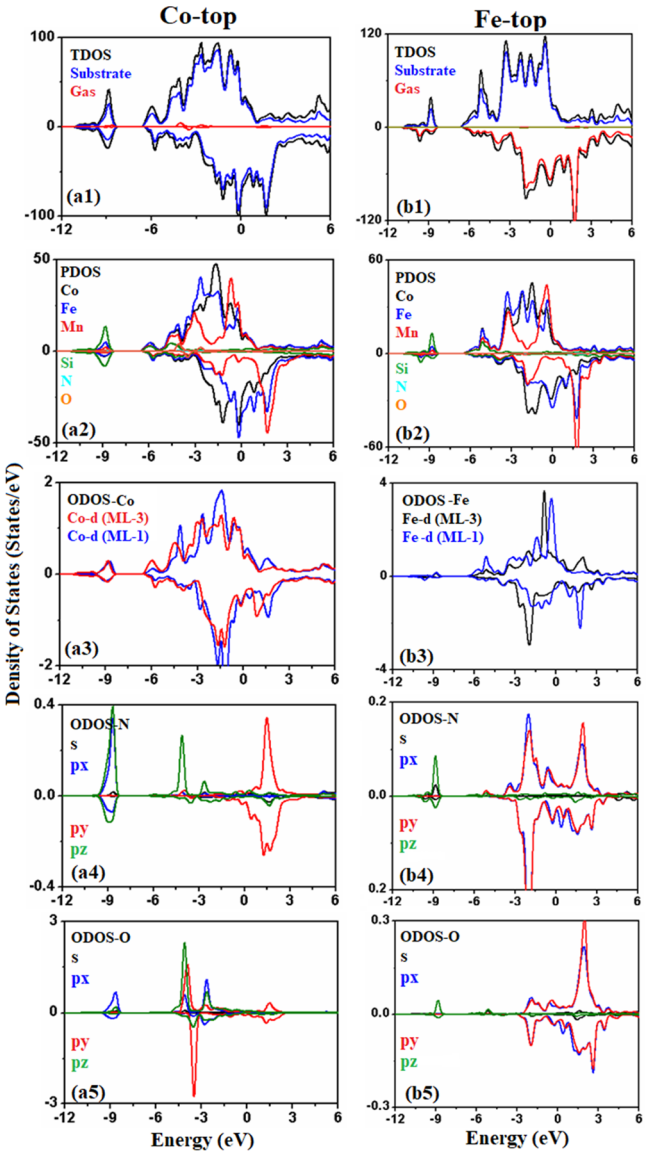

Figure 6. (a1) TDOS of NO on the top of the Co-atom of the (001) CoFeMnSi surface, (a2) PDOS of Co, Fe, Mn, Si, N, and O atoms, (a3) ODOS of the Co atom in ML-1 and ML-3, (a4) ODOS of the N atom of NO, (a5) ODOS of the O atom of NO, (b1) TDOS of NO on the top of the Fe atom of the (001) CoFeMnSi surface, (b2) PDOS of Co, Fe, Mn, Si, N, and O atoms, (b3) ODOS of the Fe atom in ML-1 and ML-3, (b4) ODOS of the N atom of NO, (b5) ODOS of the O atom of NO.

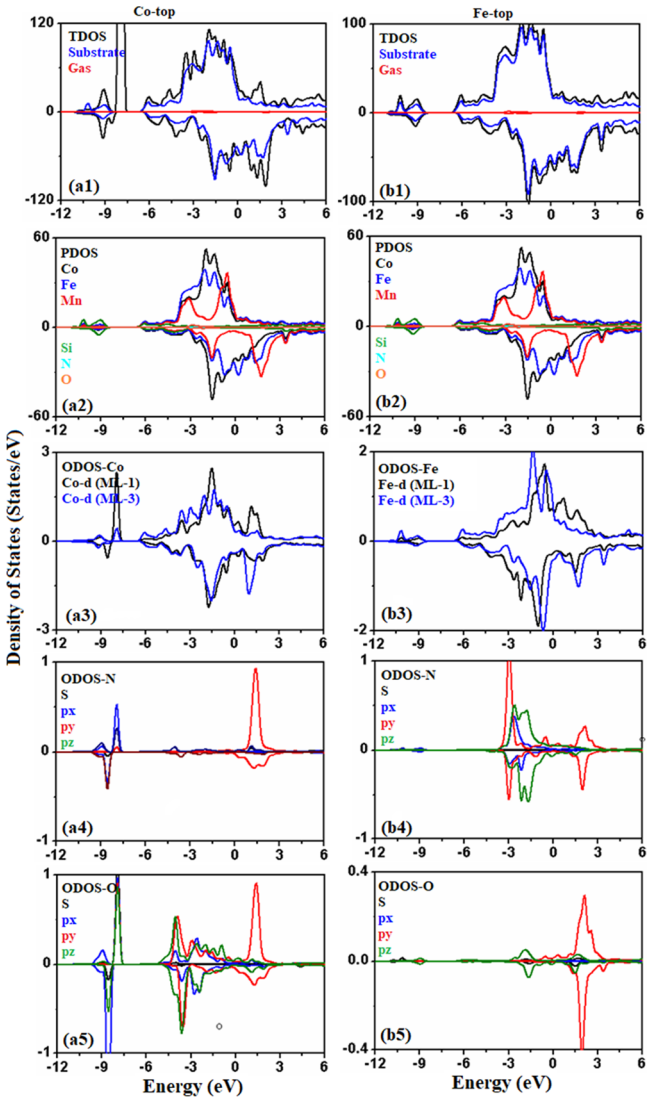

Figure 7. (a1) TDOS of NO_2 on the top of Co atom of the (001) CoFeMnSi surface, (a2) PDOS of Co, Fe, Mn, Si, N, and O atoms, (a3) ODOS of the Co atom in ML-1 and ML-3, (a4) ODOS of N atom of NO_2, (a5) ODOS of the O atom of NO_2, (b1) TDOS of NO_2 on the top of Fe atom of the (001) CoFeMnSi surface, (b2) PDOS of Co, Fe, Mn, Si, N, and O atoms, (b3) ODOS of Fe atom in ML-1 and ML-3, (b4) ODOS of the N atom of NO_2, (b5) ODOS of the O atom of NO_2.

sites, and to account for adsorption, thus, the adsorption lengths are identified.

The adsorption of gas molecules and chemical bond formation is further examined by the evaluation of the adsorption energy. The adsorption energy is −4.35, −3.18, −3.49, −6.17, and −5.12 eV for NO gas adsorbed on top of Co, Fe, Mn, Si, and hollow sites, respectively. Additionally, its value is −3.04, −2.37, −3.31, −0.08, and −3.46 eV for NO_2 gas adsorbed on A-, B-, C-, D-, and E-sites, respectively (Table 1).

The negative adsorption energy indicates that gas adsorption lowers the energy of the CFMS (001) structure because of the formation of the bonds. The results reveal that the adsorption energy for NO is generally higher than that of NO_2 with a maximum for NO adsorbed on the top of the Si atom. The adsorption of NO and NO_2 on the CFMS (001) surface is further examined using the charge transferred between gas molecule and the CFMS (001) surface, as presented in Figure 5. The figure reveals contours of charge density difference that represent a picture of the physical charge exchange. Charge is moved from the surface to the molecule through its extraction from anti-bonding states to guarantee the gas-substrate bond formation. The value of charge transferred is evaluated to be −0.30e, −0.40e, −1.24e, −2.20e, and −2.52e for NO gas adsorbed on top of Co-, Fe-, Mn-, Si-atom, and hollow site, respectively. The value of charge transferred is evaluated to 0.77e, −0.67e, −1.25e, −3.59e, and −1.03e for NO_2 gas adsorbed on the top of Co-, Fe-, Mn-, Si-atom, and hollow site, respectively (Table 1). The negative charge indicates that charge is transferred from the CFMS (001) surface to NO_x (x = 1,2) molecule. The results indicate that NO adsorbed on the

https://doi.org/10.1021/acsomega.3c00569
ACS Omega 2023, 8, 14005−14012

top of the Si atom exhibits the maximum value of charge transferred that is consistent with its evaluated adsorption energy. Whereas in adsorption of NO_2 molecules, the maximum value of charge transferred is again on the top of the Si atom site, but the adsorption energy is minimum among all other atoms. NO_2 gas has maximum adsorption energy on the hollow site. It is found that NO molecule dissociates into nitrogen (N) and oxygen (O) atoms as evidenced by the calculated distance between N and O atom d(N, O) is 3.61, 1.18, 1.39, 5.58, and 3.07 Å, respectively, for the Co-top, Fe-top, Mn-top, Si-top, and hollow-top site. However, NO_2 molecule dissociate into atomic N and O atoms only for the adsorption at the Si-top site with d(N, O) of 3.013 Å. However, for other sites, the N and O atoms of the molecule maintain their connection, and the d(N, O) value is found to be 1.35, 1.26, 1.29, and 1.33 Å, respectively, for the Co-top, Fe-top, Mn-top, and hollow-top site.

Figures 6 and 7 show the TDOS, PDOS, and ODOS of NO_x molecules adsorbed on the top of Co and Fe atoms in the ML1 of the CFMS (001) surface.

It is noticed that the adsorption of the NO_x molecule increases the population of electronic states near the Fermi level. Similar to the bare surface, the electronic states near the Fermi level mainly belong to Co and Fe atoms (in the ML1). The ODOS of Co/Fe atoms shows that the d-orbital of the atoms in the ML1 is more spin-polarized than the inner layer ones. For N and O atoms of the NO_x, we find that these atoms are highly spin-polarized after adsorption; particularly, the p-orbitals have remarkable asymmetry in two spin channels. In addition, the p-orbitals of N/O atoms are present near the Fermi level. Such a redistribution of electronic states of N/O atoms describes the presence of strong interactions between Co/Fe d-states and N/O p-states. This p−d hybridization of electronic states allows the gas molecule to interact and draw the charge from the CFMS (001) surface.

4. CONCLUSIONS

Based on density functional theory (DFT) calculations, herein, the structural, electronic, and adsorption properties of NO_x (x = 1, 2) gas molecules adsorbed the (001) surface of the CoFeMnSi quaternary Heusler alloy have been investigated in detail. The interaction of the molecules with surface was tested at various symmetry sites. The adsorption strength and its mechanism were explored with energy (E_a), magnitude of charge transfer (ΔQ), charge density difference (CDD), minimum distance between the molecule and surface (d), and electronic DOS. The results showed that both NO and NO_2 molecules are chemically adsorbed and strongly interact with the surface evidenced by the large value of E_a and ΔQ. In particular, the NO_x molecule dissociates into N and O atoms for some adsorption configurations. The Bader charge analysis reveals that NO_x molecules act as charge acceptors by drawing charge from the surface atoms through p−d hybridization. This study might play a significant role in exploring the gas sensing activity of Heusler alloys.

AUTHOR INFORMATION

Corresponding Authors

Muhammad Mushtaq − *Department of Physics, University of the Poonch Rawalakot, 12350 Rawalakot, AJK, Pakistan;* orcid.org/0000-0001-5496-2836; Phone: +92 3445864590; Email: mushtaq325@gmail.com

Shaimaa A. M. Abdelmohsen − *Department of Physics, College of Science, Princess Nourah bint Abdulrahman University, Riyadh 11671, Saudi Arabia;* Email: shamohamed@pnu.edu.sa

Authors

Norah Algethami − *Department of Physics, Faculty of Science, Taif University, Taif 21944, Saudi Arabia*

Muhammad Abdul Rauf Khan − *Department of Physics, University of the Poonch Rawalakot, 12350 Rawalakot, AJK, Pakistan*

Ahmad I. Ayesh − *Physics Program, Department of Mathematics, Statistics and Physics, College of Arts and Sciences, Qatar University, Doha 00000, Qatar;* orcid.org/0000-0002-0442-5941

Muhammad Mateen − *Provincial Key Laboratory of Solid-State Optoelectronic Devices, Zhejiang Normal University, Jinhua 321004, China*

Amel Laref − *Department of Physics and Astronomy, College of Science, King Saud University, Riyadh 11671, Saudi Arabia*

M. Khalid Hossain − *Institute of Electronics, Atomic Energy Research Establishment, Bangladesh Atomic Energy Commission, Dhaka 1349, Bangladesh*

Complete contact information is available at: https://pubs.acs.org/10.1021/acsomega.3c00569

Notes

The authors declare no competing financial interest.

ACKNOWLEDGMENTS

The authors express their gratitude to Princess Nourah bint Abdulrahman University Researchers Supporting Project number (PNURSP2023R61), Princess Nourah bint Abdulrahman University, Riyadh, Saudi Arabia.

REFERENCES

(1) You, C.; Fu, H.; Li, Y.; Ou, Z.; Ma, L.; Tian, N.; Wang, V. Fabrication and intrinsic physical property of spin-gapless like Heusler alloy CoFeMnSi single crystal. *Mater. Res. Bull.* **2021**, *133*, No. 111044.

(2) Kojima, T.; Kameoka, S.; Tsai, A.-P. Heusler alloys: A group of novel catalysts. *ACS Omega* **2017**, *2*, 147−153.

(3) Bainsla, L.; Yilgin, R.; Tsujikawa, M.; Suzuki, K.; Shirai, M.; Mizukami, S. Low magnetic damping for equiatomic CoFeMnSi Heusler alloy. *J. Phys. D: Appl. Phys.* **2018**, *51*, No. 495001.

(4) Ilkhani, M.; Yeganeh, M.; Boochani, A.; Yari, A. Electronic structure and magnetic properties of the CoFeMnZ (Z = As and Si) Heuslers by XAS, XMCD and MOKE: A DFT study. *Mater. Today Commun.* **2021**, *26*, No. 101773.

(5) Mishra, V.; Barwal, V.; Pandey, L.; Kumar Gupta, N.; Hait, S.; Kumar, A.; Sharma, N.; Kumar, N.; Chaudhary, S. Investigation of spin gapless semiconducting behaviour in quaternary CoFeMnSi Heusler alloy thin films on Si (100). *J. Magn. Magn. Mater.* **2022**, *547*, No. 168837.

(6) Mebed, A. M.; Mushtaq, M.; Faizan, M.; Neffati, R.; Laref, A.; Godara, S.; Maqbool, S. Adsorption of CO over the Heusler alloy CrCoIrGa (001) surface: first-principles insights. *RSC Adv.* **2022**, *12*, 17853−17863.

(7) Kojima, T.; Kameoka, S.; Tsai, A.-P. The emergence of Heusler alloy catalysts. *Sci. Technol. Adv. Mater.* **2019**, *20*, 445−455.

(8) Duncan, B. N.; Lamsal, L. N.; Thompson, A. M.; Yoshida, Y.; Lu, Z.; Streets, D. G.; Hurwitz, M. M.; Pickering, K. E. A space-based, high-resolution view of notable changes in urban NOx pollution

around the world (2005−2014). *J. Geophys. Res.: Atmos.* **2016**, *121*, 976−996.
(9) (a) Salih, E.; Ayesh, A. I. Enhancing the sensing performance of zigzag graphene nanoribbon to detect NO, NO2, and NH3 gases. *Sensors* **2020**, *20*, 3932. (b) Tian, B.; Ma, S.; Zhan, Y.; Jiang, X.; Gao, T. Stability and catalytic activity to NOx and NH3 of single-atom manganese catalyst with graphene-based substrate: A DFT study. *Appl. Surf. Sci.* **2021**, *541*, No. 148460.
(10) Gómez-García, M.; Pitchon, V.; Kiennemann, A. Pollution by nitrogen oxides: an approach to NOx abatement by using sorbing catalytic materials. *Environ. Int.* **2005**, *31*, 445−467.
(11) Oum, W.; Mirzaei, A.; Hussain, T.; Bang, J. H.; Han, S.; Shin, K. Y.; Yu, D. J.; Kang, S.; Kaewmaraya, T.; Kim, S. S.; et al. Room temperature NO2 sensing performance of a-C-decorated TeO2 nanowires. *Sens. Actuators, B* **2022**, *363*, No. 131853.
(12) Bae, H.; Hussain, T.; Choi, H.; Lee, H. Boron-Rich Boron Nitride Nanotubes as Highly Selective Adsorbents for Selected Diatomic Air Pollutants: A DFT Study. *Adv. Theory Simul.* **2022**, *5*, No. 2100409. (acccessed February 19, 2023).
(13) Hu, C.; Yu, X.; Li, Y.; Cheng, J.; Xiao, B. M2CS2 (M = Sc, Y) with brand-new MXene phase: The promising candidate as the N/O-containing gases sensor and/or capturer. *Appl. Surf. Sci.* **2023**, *607*, No. 155104.
(14) Deshpande, S.; Deshpande, M.; Ahuja, R.; Hussain, T. Tuning the electronic, magnetic, and sensing properties of a single atom embedded microporous C3N6 monolayer towards XO2 (X = C, N, S) gases. *New J. Chem.* **2022**, *46*, 13752−13765.
(15) Amu-Darko, J. N. O.; Hussain, S.; Gong, Q.; Zhang, X.; Xu, Z.; Wang, M.; Liu, G.; Qiao, G. Highly sensitive In2O3/PANI nanosheets gas sensor for NO2 detection. *J. Environ. Chem. Eng.* **2023**, *11*, No. 109211.
(16) Kresse, G.; Furthmüller, J. Efficient iterative schemes for ab initio total-energy calculations using a plane-wave basis set. *Phys. Rev. B* **1996**, *54*, 11169−11186.
(17) Perdew, J. P.; Burke, K.; Ernzerhof, M. Generalized Gradient Approximation Made Simple. *Phys. Rev. Lett.* **1996**, *77*, 3865−3868.
(18) Grimme, S.; Antony, J.; Ehrlich, S.; Krieg, H. A consistent and accurate ab initio parametrization of density functional dispersion correction (DFT-D) for the 94 elements H-Pu. *J. Chem. Phys.* **2010**, *132*, No. 154104. (acccessed 2020/05/28)
(19) Alijani, V.; Ouardi, S.; Fecher, G. H.; Winterlik, J.; Naghavi, S. S.; Kozina, X.; Stryganyuk, G.; Felser, C.; Ikenaga, E.; Yamashita, Y.; et al. Electronic, structural, and magnetic properties of the half-metallic ferromagnetic quaternary Heusler compounds CoFeMnZ ($Z=\text{Al}$, Ga, Si, Ge). *Phys. Rev. B* **2011**, *84*, No. 224416.

https://doi.org/10.1021/acsomega.3c00569
ACS Omega 2023, 8, 14005−14012